Mixing Characteristics of Coaxial Injectors at High Gas to Liquid Momentum Ratios

P. A. Strakey* and D. G. Talley

Air Force Research Laboratory

&

J. J. Hutt

NASA Marshall Space Flight Center

Abstract

A study of the spray of a swirl coaxial gas-liquid injector operating at high gas to liquid momentum ratios is reported. Mixing and droplet size characteristics of the swirl injector are also compared to a shear coaxial injector, currently being used in the Space Shuttle Main Engine fuel preburner. The injectors were tested at elevated chamber pressures using water as a LOX simulant and nitrogen and helium as gaseous hydrogen simulants. The elevated chamber pressure allowed for matching of several of the preburner injector conditions including; gas to liquid momentum ratio, density ratio and Mach number. Diagnostic techniques used to characterize the spray included; strobe back-light imaging, laser sheet spray imaging, mechanical patternation, and a phase Doppler interferometry. Results thus far indicate that the radial spreading of the swirl coaxial spray is much less than was reported in previous studies of swirl injectors operating at atmospheric back-pressure. The swirl coaxial spray does, however, exhibit a smaller overall droplet size which may be interpreted as an increase in local mixing.

Introduction

The fuel preburner used on the Space Shuttle Main Engine (SSME), which supplies hot, hydrogen rich gas to run the turbopump, currently employs a 264-element shear coaxial injector. Previous testing at NASA Marshall Space Flight Center has revealed temperature variations as much as 20% of the mean temperature in the hot gas supply entering the turbopump. The temperature variations, which are believed to be due to poor inter-element mixing, have been suspected to be a leading cause of turbine blade cracking problems.

Swirl injectors are believed to have increased mixing efficiency over shear coaxial injectors as a result of the radial momentum imparted to the swirling liquid sheet. A number of single and multi-element hot-fire studies have shown improved engine performance with swirl coaxial injectors over conventional shear coaxial injectors.[1-6] It has been postulated that adding swirl to the SSME preburner injectors could reduce the incidence of turbine problems through an improvement in inter-element mixing. However, most previous studies of swirl coaxial injectors have been conducted at moderate to high oxidizer to fuel mixture ratios. Very little work has been done at low mixture ratios (less than 1.0) characteristic of the SSME preburner. The gas to liquid momentum ratio is much higher at these low mixture ratios, which suggests that adding swirl to the liquid could be relatively less effective. The objective of this study is to determine the effect of swirl on the mixing efficiency of coaxial injectors at high gas to liquid momentum ratios.

Hot-fire work

Rahman et. Al[1] studied a swirl coaxial injector in a windowed combustion chamber using LOX and gH_2 at chamber pressures up to 2.4 MPa and O/F mixture ratios between 3.6 and 166. They generally found that the swirl injector produced c* efficiencies greater than 92%. Also, flame visualization showed that the swirl injector flame had a significantly larger cone angle than a similarly sized shear coaxial injector tested previously at a mixture ratio of 5.7.

Tamura et al.[2] investigated several 9-element swirl coaxial injectors using LOX/LH_2 at a chamber pressure of 3.5 MPa and mixture ratios between 4.5 and 7.5. They also tested a 9-element shear coaxial

---

* Research Scientist, AFRL/PRSA, 10 E. Saturn Blvd., Edwards AFB, CA 93524

injector for the purpose of comparison. They found that the swirl coaxial injectors produced a higher chamber wall heat load than the shear coaxial injector at axial locations close to the injector faceplate. Pressure measurements along the length of the chamber indicated that the swirl coaxial injector spray combustion zone reached the chamber walls at axial distances significantly less than the shear coaxial injector. The chamber pressure measurements also revealed that the c* efficiency for the shear and swirl coaxial injectors was similar ($c^* \approx 0.98$) for mixture ratios less than 6, but the shear coaxial injector exhibited a drop in c* efficiency for mixture ratios greater than 6 while the swirl injector c* efficiency remained constant at $c^* \approx 0.98$.

Sasaki[3] and coworkers tested a variety of swirl coaxial injectors along with a shear coaxial injector in a single element combustion chamber using LOX and gH_2 at chamber pressures of 2.6 MPa and 3.5 MPa and mixture ratios between 4.0 and 8.0. Their results were similar to those of Tamura et. al in terms of chamber heat load and chamber axial pressure distribution. Their results also indicated that an improvement in c* efficiency was realized as the mixture ratio was increased. This was attributed to an increase in spray cone angle for the swirl coaxial injectors as the fuel to oxidizer velocity ratio was decreased. They also found, however, that an increase in the fuel to oxidizer velocity ratio as a result of decreasing the fuel annulus size while holding mixture ratio constant also resulted in an increase in performance.

Obermaier[4] and coworkers studied a 94-element swirl coaxial injector using MMH and N_2O_4 at chamber pressures between 5.5 MPa and 7.1 MPa and a mixture ratio of 2.2 and found very good engine performance, with c* efficiencies between 99 % and 100 %.

Elam[5] at NASA Marshall Space Flight Center tested a 60-element swirl coaxial injector with LOX/gH_2 at mixture ratios between 5.2 and 6.9 and LOX/methane at mixture ratios between 2.6 and 3.5. Thrust chamber pressures were around 10.3 MPa for all of the tests. The results indicated that c* efficiency increased as mixture ratio was increased. The increase in efficiency was believed to be due to an increase in swirl cone spray angle as the fuel to oxidizer momentum ratio was decreased.

An extensive study was performed at Pratt and Whitney under the Air Force reusable rocket engine program (XLR129) in the early 1970's.[6] The injector selected for the engine preburner was a 253

element swirl coaxial injector burning LOX and gH_2. Swirl coaxial elements were selected for the preburner because they were believed to have increased mixing performance over a wide range of throttling conditions as compared to shear coaxial injectors. The preburner was tested at chamber pressures between 4.1 and 30.0 MPa and mixture ratios between 0.66 and 1.22. The preburner was found to have good combustion performance ($c^* > 94\%$) at all operating conditions. Temperature measurements at the preburner exit showed that the maximum radial temperature variation across the preburner was less than 3.5 % of the mean temperature.

Cold-Flow Work

A number of cold flow studies of swirl injectors using water and inert gases as simulants have been conducted to investigate the enhanced mixing capability that swirl injectors offer. Hulka and coworkers[7] measured the Rupe mixing efficiency of several swirl coaxial injectors at atmospheric back-pressure using water and a sucrose solution to simulate LOX/gH_2. They tested the injectors at a broad range of mixture ratios between 0.94 and 17.8. The fuel to oxidizer velocity ratios ranged from 1.15 to 4.28. They found that the Rupe mixing efficiency increased as the oxidizer free swirl angle increased, which is a function of injector geometry. They also found that Rupe mixing efficiency increased as the fuel to oxidizer velocity ratio was increased (O/F mixture ratio decreased).

Mehegan et al.[8] performed an extensive study of both swirled and non-swirled coaxial injectors under cold-flow conditions using water and nitrogen as simulants for LOX/gH_2 at atmospheric back-pressure. Due to the inability to match all of the important scaling parameters at atmospheric pressure, the authors scaled the flowrates to match the desired hot-fire mixture ratio conditions (MR=4.0 - 11.0), which resulted in a gas to liquid momentum ratio much higher than hot-fire conditions, but still lower than the momentum ratios studied here. Measurements of liquid and gas flux were made with a two-phase impact probe and droplet size measurements utilizing the frozen wax technique were also presented. Their results showed that the swirl injector produced a hollow cone spray, while the shear coaxial injector produced a solid cone spray. An increase in the radial spreading of the swirl injector spray was realized with an increase in the inlet swirl velocity. Their results also showed an improvement in Rupe mixing efficiency

over the conventional shear coaxial injector as a result of the induced swirl flow. Also, a significant decrease in droplet size was observed with the swirl injector which was attributed to the penetration of the annular gas flow through the radially expanding liquid sheet.

Cox[9] reported results of mechanical patternation measurements of liquid flux with a swirl coaxial injector identical to the injector studied here. Cox noted the importance of high pressure testing in order to match both the gas to liquid density ratio and velocity ratio. The results presented were, however, conducted at atmospheric back pressure due to facility limitations. Water and air were used as simulants for LOX/gH_2 and the gas to liquid velocity ratio was matched to the SSME preburner conditions. Radial patternation measurements of liquid flux indicated a hollow-cone spray pattern for the swirl injector. Comparative measurements performed with the SSME fuel preburner injector showed that the shear coaxial injector produced a spray with a very confined liquid core and relatively poor radial spreading of the spray.

Rhaman[10] performed a phase Doppler interferometry (PDI) study of a swirl coaxial injector of similar geometry to the injector studied here. Water was used as an oxidizer simulant and nitrogen, argon, and helium were used as fuel simulants at atmospheric back-pressure. The mixture ratio varied from 30.3 to 82.7 which resulted in a relatively low gas momentum. The results indicated a similitude in spray properties such as droplet size, velocity and mass flux as the gas density was varied while holding the gas to liquid axial momentum ratio constant at 0.11, which indicated that the momentum ratio played an important role in spray characteristics. Mass flux measurements indicated a hollow cone spray for all of the gas densities studied.

The hot-fire studies of swirl injectors has generally shown good engine performance, and usually an improvement over shear-coaxial injectors. Very little work has been done at the low mixture ratio conditions of the SSME preburner shear coaxial injector, in which the gas momentum is very large. Most of the previous cold-flow studies have been done at operating conditions which do not simulate many of the important scaling parameters of the injector. Although it is difficult, if not impossible, to simulate all of the scaling parameters which are known to affect the attributes of a spray, it is possible to isolate certain groups of parameters which may play an important role in certain characteristics of the spray. A number of

experimental studies have shown that both gas to liquid velocity ratio and density ratio as well as injector geometry scaling play an important role in the mixing characteristics and mass distribution of a spray.[10-14] Other studies have shown that the velocity ratio and Weber number can affect the droplet size.[10-13]

In this study, a swirl injector is investigated under back pressure conditions at flowrates which allow for matching of the injector gas to liquid: velocity ratio, density ratio, momentum ratio, and gas Mach number. Also, the current SSME preburner injector was tested for purposes of comparison. The results provide a better understanding of how swirl coaxial injectors perform at high gas to liquid momentum ratios.

Experimental Facility

The experimental investigation was carried out in the injector characterization facility at the Air Force Research Laboratory, Edwards AFB, which is capable of characterizing full scale single element rocket injectors in cold flow at pressures to 13.8 MPa. A simplified schematic of the facility is shown in Figure 1. Water, which was used as a simulant for liquid oxygen, was stored and pressurized in a 1 m^3 tank. Nitrogen, helium, or mixtures of these were stored in 6 m^3 tanks at 41.4 MPa. The injector gas and liquid flow rates were controlled with throttling valves and measured with turbine flow meters to an accuracy of +/- 1%. The maximum water flow rate was 1.8 kg/s and the maximum nitrogen and helium flow rates were 0.1 kg/s each. The chamber consists of a 0.5 m diameter stainless steel, optically accessible pressure vessel containing a 27 tube linear array mechanical patternator which can be traversed through the spray. The patternator tubes are 6.35 mm square in dimension. A mechanical shutter prevented liquid from entering the tubes until the spray conditions were obtained at which time the shutter was opened and liquid was collected for a specified amount of time in a series of stainless steel bottles connected to the patternator tubes. After the shutter has closed, the bottles were de-pressurized and the liquid was emptied into beakers and weighed. The mass flux was simply the mass of collected fluid divided by the collection time and cross sectional area of the collection tubes. For these experiments the patternator was positioned at the centerline of the injector, therefore, radial profiles of liquid mass flux were obtained. The bottles were vented to a common manifold that was routed back to the chamber to

allow venting of gas that enters the patternator tubes along with the liquid. This configuration did not, however, provide true iso-kinetic sampling and some rejection of liquid did occur at the entrance of the patternator tubes where a stagnation zone was produced by the impingement of high velocity gas on the patternator tubes. The error associated with the measurements will be discussed later.

Three 50 mm and one 120 mm sapphire window provided optical access through the chamber. Spray imaging experiments were conducted at a variety of test conditions using a 5 us duration strobelight to back-light the spray and a CCD camera and VCR to capture and store images of the spray. These images yielded qualitative information on the shape of the sprays. Experiments were also conducted using an Argon-ion laser sheet passing through the axis of the spray. An expanding light sheet was generated by a combination of a 500 mm focal length spherical lens and a 40 mm focal length cylindrical lens. The scattered laser light was collected with the CCD camera which integrates the collected light over the frame duration of 16.7 ms. The images were again recorded with a VCR. The laser light sheet provided a better means of measuring spray angles.

The injectors were mounted in manifolds which were in turn mounted on a stepper motor driven translating stage inside the chamber. The translating stage provided up to 12 cm of radial traverse for making PDI velocity and droplet size measurements. The entire injector assembly could also be traversed 14 cm axially. A schematic of injector geometry is shown in Figure 2. The shear coaxial injector had a post internal diameter of 2.26 mm, a gas gap of 1.04 mm and a post tip recess of 2.54 mm. These dimensions are equivalent to the dimensions of the SSME fuel preburner injector.[16] The swirl injector was similarly sized with tangential inlet slots for the liquid flow and a slot to exit post area ratio of 0.55.

Injector Scaling Parameters

Chamber pressures and flow rates for the cold flow tests were chosen to match the following SSME preburner injector hot fire similarity parameters: velocity ratio, density ratio, momentum ratio, mixture ratio, and Mach number. The selected test matrix is given in Table 1. Because the hot-fire conditions were based on the SSME preburner shear coaxial injector, the cold-flow conditions were designed for the shear coaxial injector. The flow conditions for the swirl injector are somewhat different due to the differences both in injector geometry and internal flow patterns.

The most notable difference between cold-flow and hot-fire conditions was the liquid Reynolds number, which was a factor of 20 less than the hot-fire conditions. The cold-flow liquid Reynolds number was lower due to the seven-fold higher viscosity of water and an injection velocity which was about three times lower than the hot fire conditions for run 1. The maximum injection velocity was limited by matching the gas Mach number and by the maximum velocity achievable without cavitating the injector for the given chamber pressure. In order to examine the effects of Reynolds number, a second set of test conditions was generated using a mixture of nitrogen and helium for the gas side. The lower density of the nitrogen/helium mixture in run 2 allowed for higher chamber pressures and higher injector flow rates without cavitation, while still maintaining injector Mach number. The net effect was a two-fold increase in the liquid Reynolds number while maintaining all of the other scaling parameters.

Swirl Injector Results

At each of the test conditions in Table 1, radial profiles of liquid mass flux were measured with the mechanical patternator at axial locations of 51, 89 and 127 mm from the injector tip. Figure 3 contains radial plots of the local liquid flowrate normalized by the injected flowrate for the swirl coaxial injector for run 1 at axial locations of 51, 89 and 127 mm. Figure 3 indicates that the liquid flowfield was not hollow-cone in nature, which is typical with swirl injectors, but rather the liquid was concentrated along the injector axis, and gradually dispersed with increasing axial distance from the injector. The accuracy of the liquid flux measurements can be assessed by the collection efficiency which is defined as the integrated flux normalized by the injected flowrate. The collection efficiency calculated for the data in Figure 3 is listed in the third column of Table 2. It is interesting to note that the collection efficiency was greater than one at axial locations of 51 mm and 89 mm, indicating that more liquid was collected than injected. This is believed to be an artifact of the limited measurement resolution which provided few data points for integration resulting in an overestimation of the integrated fluxes. The problem is most evident at the axial location of 51 mm where most of the collected liquid fell within the three central patternator tubes.

Measurements of flowfield axial velocity were made with a PDI at axial locations of 51 and 89 mm. Measurements at 127 mm were not possible due to optical accessibility limitations within the

chamber. The PDI was optically configured to measure the smallest droplets possible. It was calculated that droplets less than about 7 um in diameter would be following the mean flowfield completely as defined by a Stokes number greater than ten, and could be used as "seed" particles for making measurements of the gas phase velocity. The Stokes number is defined as;

$$St = \frac{\tau_F}{\tau_D} \qquad \text{(Eq. 1)}$$

where τ_F is the time scale of the flowfield and τ_D is the droplet response time which are calculated as follows.

$$\tau_F = \frac{Z}{V} \qquad \text{(Eq. 2)}$$

$$\tau_D = \frac{\rho_l \cdot D^2}{18 \cdot \mu_g} \qquad \text{(Eq. 3)}$$

In Equation 2, Z is the minimum distance from the injector and V is the maximum flowfield velocity. For the present experiments the minimum distance from the injector, Z, was 51 mm and the maximum flowfield velocity was estimated to be 35 m/s from initial experiments. This yielded a time constant of 1.45 ms and a maximum droplet size of 7 um for a Stokes number of ten.

The gas velocity profiles, as shown in Figure 4, show that the peak flow occurred along the injector axis similar to the liquid flux. This provides for a relatively uniform mixture ratio distribution within the element flow pattern, but would not promote good inter-element mixing when a number of these elements are arranged in an array such as the SSME preburner.

Discharge coefficient measurements revealed that C_d was 0.25, which is close to the theoretical discharge coefficient for a hollow core flow of 0.28, indicating that a stable gas core existed within the liquid post. This suggests that the liquid mass distribution was hollow cone in nature at the exit of the injector. It is postulated that at the low mixture ratio studied here, the momentum of the gas stream collapsed the swirling liquid sheet into a confined liquid stream, which resulted in a liquid mass distribution characteristic of a shear coaxial injector, with peak fluxes occurring along the injector axis and relatively little radial spreading of the liquid phase.

Most of the previous cold-flow swirl injector studies, which have shown a hollow cone spray, have been done at either high mixture ratios or at atmospheric back-pressure conditions which cannot match the gas to liquid density ratio. In Figure 5 a comparison is presented between data collected in the present study and data collected by Cox[9] at atmospheric back-pressure for the same injector geometry. In both cases the gas to liquid velocity ratio was matched to the SSME preburner hot-fire conditions. The data presented by Cox is plotted as local mass flow normalized by an arbitrary scaling constant, therefore only qualitative comparisons can be made. The hollow cone spray observed by Cox became solid cone in nature at the higher gas densities studied here.

Momentum Ratio Effects

In order to understand why the swirl injector showed such poor radial spreading at the high gas to liquid momentum ratios studied here, a series of experiments was performed in which the liquid flowrate through the injector was held constant and the gas flowrate was gradually increased, while maintaining a constant back-pressure of 2.97 MPa. This allowed for a variation in momentum ratio while maintaining the density ratio at a constant value. A strobelight was used to back-light the spray and a CCD camera was used to capture the images which were stored on a VCR. The strobelight was then replaced with an argon-ion laser sheet passing through the axis of the spray, while again using a CCD camera and VCR to capture and store the images. Figure 6 is a series of images from the spray at increasing gas momentum, from left to right. The top series of images are the strobe back-lit images while the bottom series was obtained with the laser sheet. The strobelight images provide qualitative information about the shape of the spray, while the laser sheet images allow for more accurate measurement of the spray cone angle, which was measured as the angle between the areas of peak scattering intensity at the exit of the injector. As can be seen in the images, the spray, which was hollow cone in nature at the lower gas momentum, appears to collapse to a solid cone spray at the highest gas momentum (rightmost image), which corresponded to the conditions of run 1.

Swirl Injector Modeling

In an effort to model the effect of the high momentum gas stream on the swirling liquid sheet, a momentum balance analysis was performed for the swirl injector. A schematic of the injector flow and associated notation is given in Figure 7. For a swirl injector in the absence of a co-annular gas flow, the resulting spray half angle has been shown to be equal to the arc-tangent of the liquid radial to axial velocity ratio.[16]

$$\theta_{1/2} = \tan^{-1}\left(\frac{V_r}{V_x}\right) \qquad \text{(Eqn. 4)}$$

Since Equation 4 is actually derived from a momentum balance between the radial and axial components of liquid momentum, it is proposed here that the effect of the co-annular gas momentum can be linearly superimposed on the liquid momentum balance. With the assumptions of uniform pressure in the unconfined flow after the exit of the injector and negligible gravitational effects, the mean angle of the resultant stream can be calculated by applying a momentum balance in the axial and radial directions. Conservation of momentum in the axial direction is written as follows;

$$\dot{m}_l V_{l,x} + \dot{m}_g V_{g,x} = \dot{m}_s V_{s,x} \qquad \text{(Eqn. 5)}$$

where the resultant spray mass flowrate, $\dot{m}_s$, is equal to the sum of the mass flowrates of the gas and liquid stream. Conservation of momentum in the radial direction is written as follows.

$$\dot{m}_l V_{l,r} + \dot{m}_g V_{g,r} = \dot{m}_s V_{s,r} \qquad \text{(Eqn. 6)}$$

Since the radial velocity component of the gas side is zero, the radial to axial velocity ratio for the resultant spray is then;

$$\frac{V_{s,r}}{V_{s,x}} = \frac{\dot{m}_l \cdot V_{l,r}}{\dot{m}_l \cdot V_{l,x} + \dot{m}_g \cdot V_{g,x}} \equiv Mom_{r/x} \qquad \text{(Eqn. 7)}$$

where the ratio of liquid-radial momentum to total-axial momentum is denoted $Mom_{r/x}$.

The resultant spray half angle, as defined from the axis of the injector, is calculated as in Eqn.4.

$$\theta_{1/2} = \tan^{-1}\left(\frac{V_{s,r}}{V_{s,x}}\right) \qquad \text{(Eqn. 8)}$$

This approach is similar to the momentum balance approach for calculating spray angle from the impingement of two liquid streams generated by impinging type liquid rocket injectors.[17]

The gas side velocity was calculated as the bulk flow velocity in the annular region, but to calculate the liquid sheet momentum, the liquid film thickness at the exit of the injector must be known. The film thickness can be estimated from the inviscid flow theory as outlined by Yule and Chin.[18] For an injector with constant post diameter, as is the case here, the liquid film thickness is found only to be a function of the slot to post area ratio, A_s/A_o, which is equal to 0.55. This yields a film thickness, t, of 284 um and a discharge coefficient, C_d, of 0.276. For the liquid flow rate of run 1, the liquid sheet axial velocity is calculated to be 12.5 m/s and the tangential velocity is calculated to be 7.1 m/s. The tangential momentum is assumed to be completely converted to radial momentum after the liquid leaves the confinement of the post.

Without the co-annular gas flow, the radial to axial velocity ratio is 0.57 and the resultant half angle calculated by Eqn. 4 is 29.6°. The measured half angle was 26.9°, which is slightly less than the predicted half angle. This is due to frictional effects in the injector post and has been observed by others.[3]

At the conditions of run 1, the gas velocity, V_g, is 64.4 m/s, which yields a liquid-radial to total-axial momentum ratio, $Mom_{r/x}$, of 0.085 and a spray half angle, $\theta_{1/2}$, of 4.9° as calculated by Eqn. 8. This is consistent with the spray half angle as shown in Figure 6 (rightmost image), which is measured to be about 5°. It is believed that the relatively high axial momentum of the gas flow prevented the swirling liquid sheet from radially expanding.

The experimentally measured spray half angle is plotted as a function the liquid-radial to total-axial momentum ratio, $Mom_{r/x}$ in Figure 8. Also shown in Figure 8 is data collected in a similar series of experiments conducted at atmospheric chamber pressure along with a plot of Eqn. 8 which has no chamber pressure dependence. The spray angle decreases with increasing gas momentum (decreasing $Mom_{r/x}$) due to the axial gas flow acting on the radially expanding liquid sheet. The spray angle calculated with Eqn. 8 approaches zero as the momentum ratio, $Mom_{r/x}$ approaches zero, while the actual spray angle exhibited a minimum spray angle of about 4°. The minimum spray angle is a result of the deceleration and expansion of the gas jet after leaving the injector which the momentum balance does not account for. The measured spray half angles were somewhat less than the momentum balance prediction. This is believed to be due to frictional losses in the post as was observed in the case without the co-annular gas flow. It is also of

interest to note that there appears to be very little effect of chamber pressure on spray angle as seen in Figure 8. It should be pointed out that spray angle is defined as the initial spray angle as measured very close to the injector face (Z=5 mm). An effect of chamber pressure was observed when the spray angle was measured further downstream, with the higher chamber pressure resulting in a significantly smaller spray half angle. This effect is illustrated in Figure 9, which shows two images of the swirl coaxial spray operating at a momentum ratio, $Mom_{t/x}$, of 0.30 and at chamber pressures of 2.97 MPa and 0.11 MPa. Although the cone angles measured near the exit of the injector were the same, the high back-pressure spray resulted in a cone angle which decreased with axial distance from the injector, while the low back-pressure case resulted in a spray with a nearly constant cone angle. A decrease in spray cone angle with increasing back-pressure was also observed by Ortman and Lefebvre[19] and by DeCorso and Kemeny[20] in studies of pressure-swirl atomizers in the absence of a co-annular gas flow. According to DeCorso and Kemeny, entrainment of ambient chamber gas was believed to increase the local pressure outside of the spray cone that forced the spray toward its axis resulting in a decreased cone angle. The pressure gradient across the spray boundary was believed to be proportional to the chamber gas density and was confirmed by static pressure measurements inside and outside of the spray cone. The pressure difference increased with increasing chamber gas density accompanied by a reduction in spray cone angle as measured with a patternator 114 mm downstream of the injector. They also noted that the spray angle measured at the exit of the injector was independent of chamber gas density as was observed here (Fig. 8).

Integrated gas flux measurements in the present study indicated that the total gas flux was about four times greater than the injected mass flowrate at an axial location of 51 mm and about seven times greater than the injected flowrate at an axial location of 89 mm for run 1. This would indicate that the majority of the gas flowfield is entrained gas that would create a lower pressure inside of the spray cone and decrease the cone angle.

Comparison to Shear Coaxial Injector

As a point of reference in which to compare the mixing characteristics of the swirl coaxial injector, a shear coaxial injector of the type used in the SSME fuel preburner was tested at the flowrates of

run 1. The patternator was used to make measurements of liquid flux as a function of axial and radial position in the spray as was done with the swirl injector. In an effort to increase the resolution of the patternator, the patternator was stepped through the spray at 1.59 mm increments, which is one-quarter of the tube size, which increases the number of measurement points. Figure 10a is a plot of local mass flow normalized by the injected mass flow for both injectors at an axial location of 51 mm. The two injectors appear to have almost identical liquid mass flux distributions despite significant differences in injector geometry and internal flow patterns (swirl and non-swirl). As was discussed in the previous section, the high gas momentum collapsed the swirling liquid sheet into a confined liquid stream, which resulted in a spray pattern much like the shear coaxial injector. Also, with the higher number of measurements points, the integrated mass fluxes dropped significantly due to improvements in integration resolution. The collection efficiency, C_{eff}, calculated from the higher resolution measurements decreased to 0.81 and 0.86 for the swirl coaxial and shear coaxial injectors respectively. A collection efficiency less than one is expected due to non iso-kinetic sampling conditions which can be described as the rejection of the smaller droplets at the entrance of the patternator tubes due to the high flowfield velocity which creates a large stagnation pressure at the tube inlet. The small droplets tend to follow the streamlines around the patternator, while the larger droplets possess enough momentum to pass through the streamlines and into the patternator tubes. Radial plots of the liquid mass flux at the axial locations of 89 and 127 mm using the lower patternator resolution are shown in Figure 10b and Figure 10c respectively. The liquid flux distributions appear almost identical even at the farthest axial location. Collection efficiency, C_{eff}, for both injectors is given in Table 2.

Similar results for the axial velocity distribution as obtained with the PDI are shown in Figure 12, which are radial plots of the measured axial velocity for the axial locations of 51 mm and 89 mm. The gas-phase velocity distributions for the two injectors were almost identical and spread slowly in the radial direction as axial distance was increased.

Reynolds Number Variation

Due to the expense of helium associated with the relatively high flowrates used in this study, the investigation into the effects of Reynolds number was only conducted for the shear coaxial injector.

Results for the higher Reynolds number test (run 2) are presented in Figures 12 and 13 along with the results for run 1. Both results are with the shear coaxial injector, with the only difference being an increase in liquid jet and gas side Reynolds numbers as a result of using the helium/nitrogen mixture at a higher chamber pressure and flowrates. All of the other scaling parameters were maintained at the conditions listed in Table 1. Figure 12 is a radial plot of local liquid flow normalized by the injected flowrate for the two test cases. Although the shape of the distributions is similar, integrated flux calculations, which are given in Table 2, indicated that the measured liquid fluxes for run 2 were about 30% less than run 1. This is believed to be due to the higher velocities of run 2, which created larger stagnation pressures at the patternator inlet and caused an increased fraction of the droplets to flow around the patternator. The uncertainty in the integrated measurement was largest at the axial location of 51 mm, where the spatial resolution was poor and the trapazoidal integration technique employed here overestimated the integrated flux.

Figure 13 is a plot of the gas phase velocity, as measured with the smallest droplets, normalized by the injected gas velocity for the shear coaxial injector for runs 1 and 2 at axial locations of 51 and 89 mm. The normalized velocity profiles for the two test cases are very similar, even though the injection velocity for run 2 was twice that of run 1. It would appear that the normalized gas flowfield, as with the liquid mass distribution, is independent of Reynolds number, within the range of Reynolds number studied here. This is analogous to the self-preserving velocity distribution of axi-symmetric turbulent jets in which the shape of the velocity profile (after several diameters downstream) is independent of the injection velocity.

Droplet Sizing Results

Results thus far show no difference between the shear and swirl coaxial injectors based on more "macroscopic" measures such as gas and liquid mass flux distribution. In an effort to examine the effect of injector design on the local or "microscopic" mixing properties of the two sprays, the PDI was reconfigured to measure the larger particles of the spray field in an attempt to quantify the volume mean diameter, D_{30}. The test conditions for these measurements was the same as for run 1 of the mixing experiments. Although the Weber number based on liquid properties and velocity difference was

significantly lower than the actual hot-fire conditions as a result of the higher surface tension of water, qualitative information on the effect of injector design on the droplet size can still be ascertained.

Due to the optically dense nature of these sprays at the high chamber pressures studied here, a flow splitter was employed to physically separate the central core of the spray from the remainder of the spray. The flow splitter allowed only the central 2.5 mm of the spray to pass unobstructed. Measurements of the velocity field were made with and without the flow splitter, and very little difference in axial velocity was seen. A more detailed investigation of the flow splitter has been published elsewhere.[21] Figure 14 is a plot of D_{30} for both the shear coaxial and swirl coaxial injector for run 1 at an axial location of 51 mm from the injector face. It is clear from the figure that there was a significant difference in mean droplet size between the two injectors. In conjunction with the previous results which showed a similar radial distribution of liquid and gas mass flux for the two injectors, the smaller droplet size measured with the swirl coaxial injector would imply that the swirl injector spray was more uniformly mixed on a local or "microscopic" scale. The term microscopic is used to refer to a control volume located somewhere in the spray which is of a size much smaller than the spray, but is large enough to contain a significant number of droplets. The decrease in droplet size results in a larger number of smaller droplets, which would be randomly distributed in the control volume, providing a more uniform mixture ratio throughout the control volume and thus increased mixing on a microscopic scale.

Summary and Conclusions

A swirl coaxial injector and a similarly sized shear coaxial injector were tested at cold-flow conditions scaled to the SSME fuel preburner hot-fire conditions. This was accomplished by using a high back-pressure environment in order to match the injector gas to liquid; density ratio, velocity ratio, mixture ratio and momentum ratio, along with gas Mach number. The low operating mixture ratio, which resulted in a high injector gas mass flux, forced the swirling liquid sheet to collapse into a confined liquid stream. The resulting spray was found to have a relatively poor rate of radial spreading, almost identical to the shear coaxial injector which was tested at the same flowrates. A momentum balance was performed to model the effects of the high momentum coaxial gas flow on the swirl angle of the resulting spray. The

model did a reasonable job of predicting the decrease in spray angle as the gas to liquid momentum ratio was increased, which was confirmed by experimentation.

Reynolds number effects were investigated by increasing the flowrates through the shear coaxial injector using a mixture of nitrogen and helium at a higher chamber pressure. The liquid mass distribution and gas velocity profiles were found to be self similar, with very little change in the shape of the distributions from the lower Reynolds number case.

Measurements of droplet size for the two injectors revealed that the swirl coaxial injector produced a droplet size much smaller than the shear coaxial injector at the same flowrates. This is believed to be due to the increased interaction between the swirling liquid sheet and the coaxial gas flow. The smaller droplet size suggested that the swirl coaxial spray was more uniformly mixed on a local, or microscopic scale. In extrapolating to a multi-element injector, one might speculate that the swirl injector studied here may not increase inter-element mixing significantly, possibly even reducing it slightly due to the inability of smaller droplets to cross shear layers. Performance might nevertheless be improved, however, due to the smaller drop sizes. Inter-element mixing could be enhanced by increasing the amount of liquid swirl or by reducing the gas velocity which would increase the cone angle of the spray.

Acknowledgment

The authors would like to thank Mr. Mike Griggs for his assistance in the operation of the facility and in collecting the experimental data.

References

1. S. A. Rahman, S. Pal and R. J. Santoro, "Swirl Coaxial Atomization: Cold-Flow and Hot-Fire Experiments", AIAA 95-0381, 33rd Aerospace Sciences Meeting and Exhibit, January 9-12, 1995.

2. M. Sasaki, H. Sakamoto, M. Takahashi, T. Tomita and H. Tamura, "Comparative Study of Recessed and Non-Recessed Swirl Coaxial Injectors", AIAA 97-2907, 33rd Joint Propulsion Conference and Exhibit, July 6-9, 1997.

3. H. Tamura, H. Sakamotot, M. Takahashi, M. Sasaki, T. Tomita and R. Nagao, "LOX/LH2 Subscale Swirl Coaxial Injector Testing" AIAA 97-2906, 1997.

4. G. Obermaier, G. Taubenberger and D. Feyhl, "Coaxial Injector Development for Storable Propellant Upper Stage Turbopump Engines", AIAA 97-3905, 1997.

5. S. K. Elam, "Subscale LOX/Hydrogen Testing with a Modular Chamber and a Swirl Coaxial Injector" AIAA 91-1874, 1991.

6. R. Atherton, "Air Force Reusable Rocket engine Program", XLR129-P-1 Final Report AFRPL-TR-71-1, Pratt and Whitney, Vol. 1, 1971.

7. J. Hulka, J. A. Schneider and J. Davis, "Single element Injector Testing for STME Injector Technology", AIAA 92-3281, 28th Joint Propulsion Conference and Exhibit, July 6-8, 1992.

8. P. F. Mehegan, D. T. Campbell and C. H. Scheuerman, "Investigation of Gas-Augmented Injectors: Final Report", NASA CR-72703, Rocketdyne, Sept. 1970.

9. G. B. Cox, "Rocket Engine Injection Element Characterization", AIAA-88-3135, 24th Joint Propulsion Conference, Boston, July, 1988.

10. S. A. Rhaman "Primary Atomization Study of a Swirl Coaxial Liquid Propellant Rocket Injector", PhD Thesis, The Pennsylvania State University, Dept. of Mechanical Engineering, 1997.

11. A. Ferrenberg and V. Jaqua, "Atomization and Mixing Study Interim Report" NAS8-34504, Rocketdyne, July, 1983.

12. H. Gomi, "Pneumatic Atomisation with Coaxial Injectors: Measurements of Drop Sizes by the Diffraction Method and Liquid Phase Fraction by the Attenuation of Light", NAL-TR-888T, 1986.

13. R.J. Burick, "Atomization and Mixing Characteristics of Gas/Liquid Coaxial Injector Elements", Journal of Spacecraft and Rockets, Vol. 9, No. 5, pp. 326-331, May, 1972.

14. W. H. Nurick and R. M. McHale, "Noncircular Orifice Holes and Advanced Fabrication Techniques for Liquid Rocket Injectors : Comprehensive Program Summary Report", NASA CR-R9271, May, 1974.

15. M. Glogowski and M. M. Micci, "Shear Coaxial Injector Spray Characterization Near the LOX Post Tip Region", AIAA 95-2552, 1995.

16. N. Dombrowski and D. Hasson, "The Flow Characteristics of Swirl (Centrifugal) Spray Pressure Nozzles with Low Viscosity Liquids", AIChE Journal, Vol. 15, No. 4, pp. 604-611, July, 1969.

17. G. P. Sutton, *Rocket Propulsion Elements*, 6th edition, pg. 305, Wiley, New York,1992.

18. A. J. Yule and J. J. Chinn, "Swirl Atomizer Flow: Classical Inviscid Theory Revisited", ICLASS-94, Paper 111-1, pp. 334-341, Rouen, France, July, 1994.

19. J. Ortman and A.H. Fefebvre "Fuel Distributions form Pressure-Swirl Atomizers", J. Propulsion, Vol. 1, No. 1, pp. 11-15, Jan.-Feb., 1985.

20. S. M. De Corso and G. A. Kemeny, "Effect of Ambient and Fuel Pressure on Nozzle Spray Angle", ASME Transactions, Vol. 79, No. 3, pp. 607-615, 1957.

21. P.A. Strakey, D.G. Talley and W.D. Bachalo, "Phase Doppler Measurements in Dense Sprays", ILASS Americas '98, Sacramento, pp. 291-295, May, 1998.

Nomenclature

A_o	post exit area (m^2)	**Subscriprts**	
A_s	total slot area (m^2)	g	gas
c*	c-star efficiency	l	liquid
C_d	discharge coefficient	r	radial
C_{eff}	patternator collection efficiency	s	spray
D	droplet size (um)	x	axial
D_{30}	volume mean droplet diameter (um)	**Greek**	
$\dot{m}$	mass flowrate (kg/s)	ρ	density (kg/m^3)
$Mom_{r/x}$	liquid-radial to total-axial momentum ratio	$\theta_{1/2}$	spray cone half angle (deg)
P_c	chamber pressure (MPa)	τ_D	droplet response time (s)
t	liquid film thickness (um)	τ_F	timescale of flowfield (s)
V	velocity (m/s)	μ	viscosity ($N \cdot s/m^2$)
Z	axial distance from injector exit (mm)		

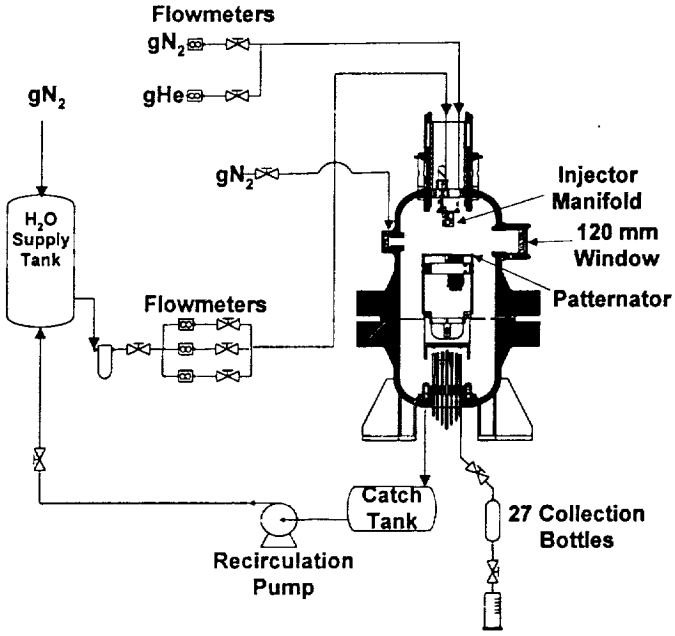

Figure 1: Facility schematic.

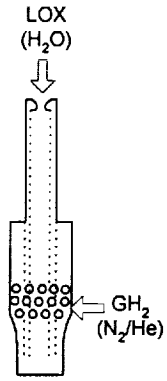

Figure 2: Schematic of shear coaxial injector.

Table 1 : Test matrix, based on shear-coaxial geometry

	SSME Preburner injector 104% Power Level	Run 1	Run 2
Chamber Pressure (MPa)	33.2	2.96	10.3
gN_2 mass fraction	-	1.0	0.61
Liquid Flow rate (kg/s)	. 108 (LOX)	.033 (H_2O)	.065 (H_2O)
Gas Flow rate (kg/s)	.116 (gH_2)	.035 (gN_2)	.070 (gN_2+gHe)
Exit Mach #	.25	.26	.26
Liquid Reynolds #	3.8×10^5	1.6×10^4	3.2×10^4
Gas Reynolds #	2.6×10^6	3.7×10^5	6.4×10^5
Momentum Ratio (Liq/Gas)	.079	.079	.079
Velocity Ratio (Liq/Gas)	.085	.084	.084
Density Ratio (Liq/Gas)	29.2	29.4	29.4
Mixture Ratio (Liq/Gas)	.930	.930	.930

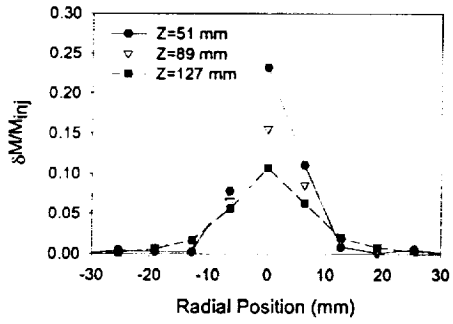

Figure 3: Radial profiles of normalized liquid mass flux for the swirl injector, run 1.

Table 2: Patternator collection efficiency, C_{eff}.

	Run 1		Run 2	
Z(mm)	Swirl	Shear Coax	Swirl	Shear Coax
51	1.27	1.33	-	0.98
89	1.23	1.18	-	0.77
127	1.08	0.99	-	0.65

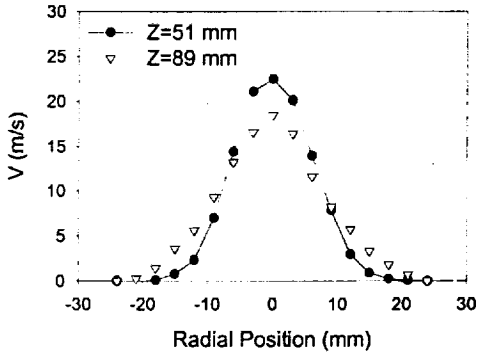

Figure 4: Radial profiles of gas phase axial velocity for the swirl injector, run1 .

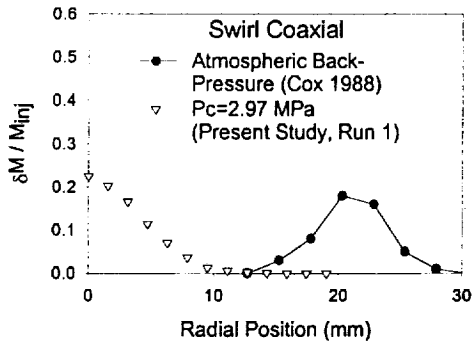

Figure 5: Comparison of present data (Pc=2.97 MPa) to that of Cox (1988, atmospheric) for the swirl injector at equal velocity ratios, Z=51 mm.

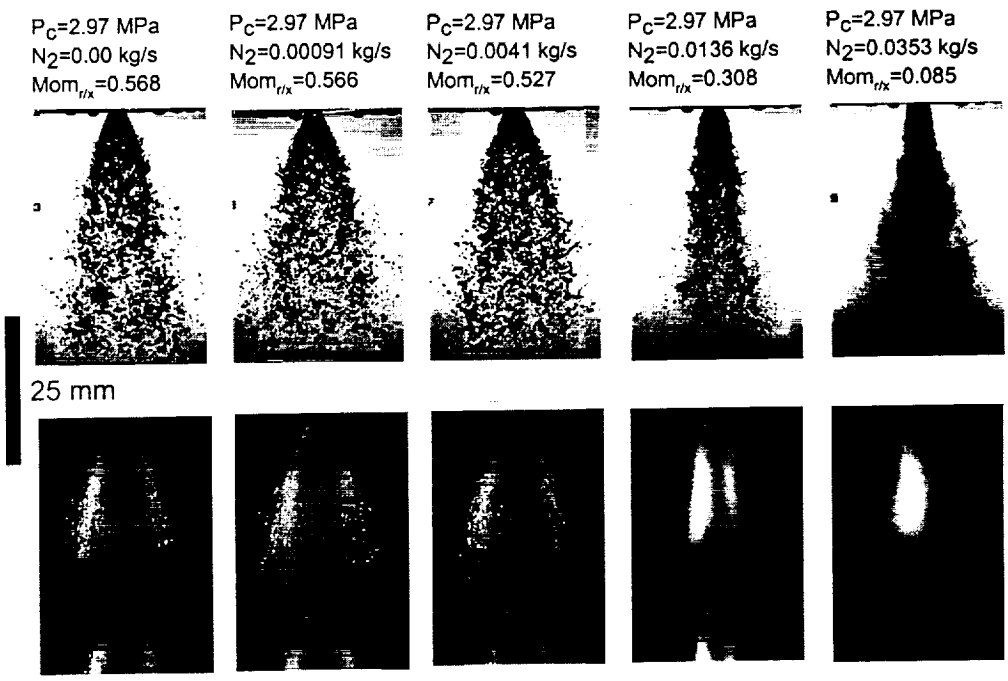

Figure 6: Strobe backlit images (top row) and laser light sheet images (bottom row) of the swirl injector spray with increasing gas momentum (left to right). At a chamber pressure of 2.97 MPa

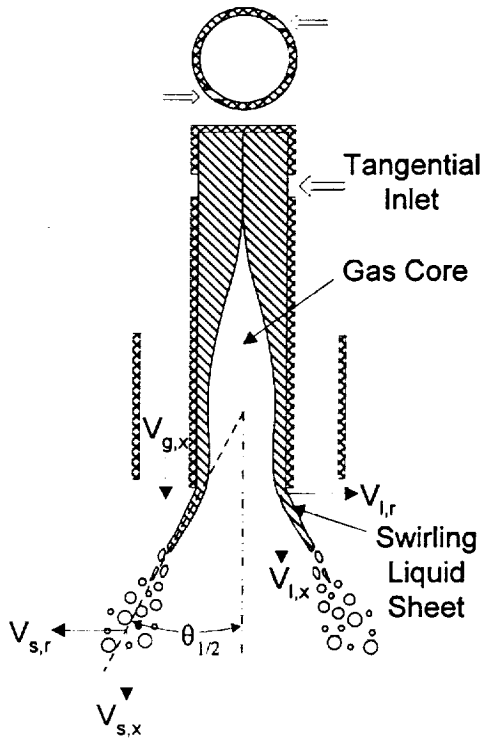

Figure 7: Schematic of swirl injector flow and associated notation.

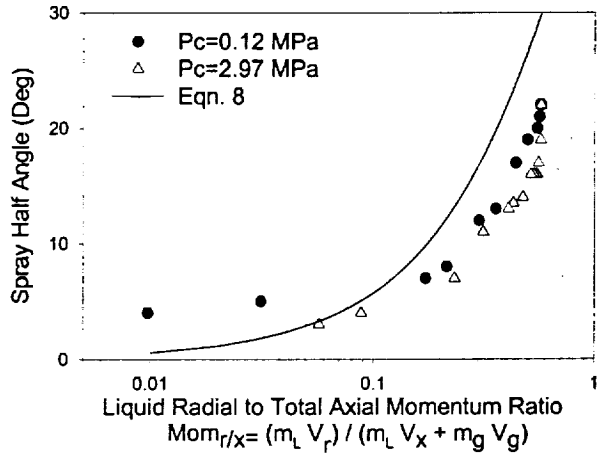

Figure 8: Spray half angle verses liquid-radial to total-axial momentum ratio.

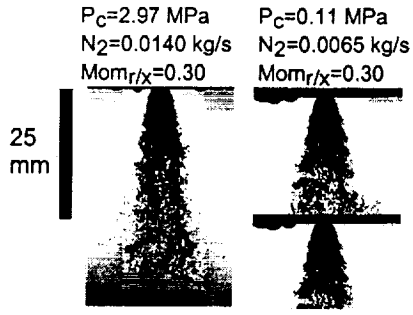

Figure 9: Strobe backlit images of swirl injector spray at equivalent momentum ratios and chamber pressure of 2.97 MPa (left) and 0.11 MPa (right).